The EMBO Journal Vol.19 No.4 pp.572–580, 2000

Op18/stathmin caps a kinked protofilament-like tubulin tetramer

Michel O.Steinmetz[1], Richard A.Kammerer[2], Wolfgang Jahnke[3], Kenneth N.Goldie[4,5], Ariel Lustig[2] and Jan van Oostrum[1]

Functional Genomics Area, Protein Sciences Unit and [3]Core Technology Area, Analytics and Biomolecular Structures, Novartis Pharma AG, CH-4002 Basel, [2]Department of Biophysical Chemistry and [4]M.E. Müller Institute for Microscopy, Biozentrum, University of Basel, CH-4056 Basel, Switzerland

[5]Present address: European Molecular Biology Laboratories, D-69117 Heidelberg, Germany

[1]Corresponding authors
e-mail: jan.van_oostrum@pharma.novartis.com

Oncoprotein 18/stathmin (Op18), a regulator of microtubule dynamics, was recombinantly expressed and its structure and function analysed. We report that Op18 by itself can fold into a flexible and extended α-helix, which is in equilibrium with a less ordered structure. In complex with tubulin, however, all except the last seven C-terminal residues of Op18 are tightly bound to tubulin. Digital image analysis of Op18:tubulin electron micrographs revealed that the complex consists of two longitudinally aligned α/β-tubulin heterodimers. The appearance of the complex was that of a kinked protofilament-like structure with a flat and a ribbed side. Deletion mapping of Op18 further demonstrated that (i) the function of the N-terminal part of the molecule is to 'cap' tubulin subunits to ensure the specificity of the complex and (ii) the complete C-terminal α-helical domain of Op18 is necessary and sufficient for stable Op18:tubulin complex formation. Together, our results suggest that besides sequestering tubulin, the structural features of Op18 enable the protein specifically to recognize microtubule ends to trigger catastrophes.

Keywords: electron microscopy/microtubule catastrophe factor/structure analysis/tubulin capping protein/tubulin-GDP-directed conformational change

Introduction

Oncoprotein 18/stathmin (referred to as Op18) is an evolutionarily well conserved 17 kDa cytoplasmic phosphoprotein (for a review see Sobel, 1991). Op18 is highly expressed in a wide variety of cancers and its high abundance seems to be necessary for the maintenance of the transformed phenotype (see Lawler, 1998, and references therein). The expression and phosphorylation levels of Op18 are regulated in response to a variety of signals that affect the state of proliferation or differentiation of different cell types including neurons (Sobel, 1991).

Op18 has only recently been found to be a factor that destabilizes microtubules (MTs), polymers of α- and β-tubulin subunits, by promoting catastrophes (referred to as the depolymerization or shrinkage phase of individual MTs; Belmont and Mitchison, 1996a). Subsequent studies have shown that phosphorylation of Op18 both *in vivo* and *in vitro* completely blocks its MT-destabilizing effect and prevents MT disassembly (Di Paolo *et al*., 1996; Horwitz *et al*., 1997; Larsson *et al*., 1997; Melander Gradin *et al*., 1997, 1998). In view of these results, Op18 is now considered to be a phosphorylation-controlled general physiological regulator of MT dynamics.

However, the mechanism by which Op18 destabilizes MTs is currently under debate. Curmi *et al*. (1997) and Jourdain *et al*. (1997) proposed that Op18 acts solely by sequestering α/β-tubulin heterodimers without interacting with MT ends as previously suggested by Belmont and Mitchison (1996a). Howell *et al*. (1999), using Op18 deletion mutants, were able to separate the tubulin-sequestering and MT catastrophe-promoting activities of the protein *in vitro*, and Larsson *et al*. (1999a,b) demonstrated that beside these two activities, Op18 also modulates tubulin's GTP metabolism. These latter studies indicate that Op18 mediates intrinsic multiple region-specific tubulin- and MT-directed regulatory activities besides sequestering tubulin dimers.

Since only very little structural information on Op18 and on the Op18:tubulin complex is available, we have performed a detailed biophysical and structural study to gain new insights into the mechanism of action of the molecule. For this purpose, we have cloned the human Op18 gene from a fetal brain cDNA library and expressed it in *Escherichia coli*. Circular dichroism (CD) spectroscopy, nuclear magnetic resonance (NMR) spectroscopy, analytical ultracentrifugation (AUC) and electron microscopy (EM) were used to examine the content of secondary structure, the oligomerization state and the molecular shape of the Op18 protein. NMR spectroscopy of [^{15}N]Op18:tubulin complexes allowed the identification of Op18 residues that do not interact with tubulin. Scanning transmission electron microscopy (STEM), in combination with digital image processing, was applied to characterize the structure of the Op18:tubulin complex in detail. Furthermore, deletion mapping of Op18 was performed to investigate the function of the C-terminal α-helical domain and the N-terminal portion of the molecule. Our approach revealed structural properties of Op18 which suggest that the protein can specifically recognize MT ends. The proposed mechanism of action of Op18 differs from the one proposed for the Kin I kinesins and katanin, which represent the other classes of known MT destabilization factors.

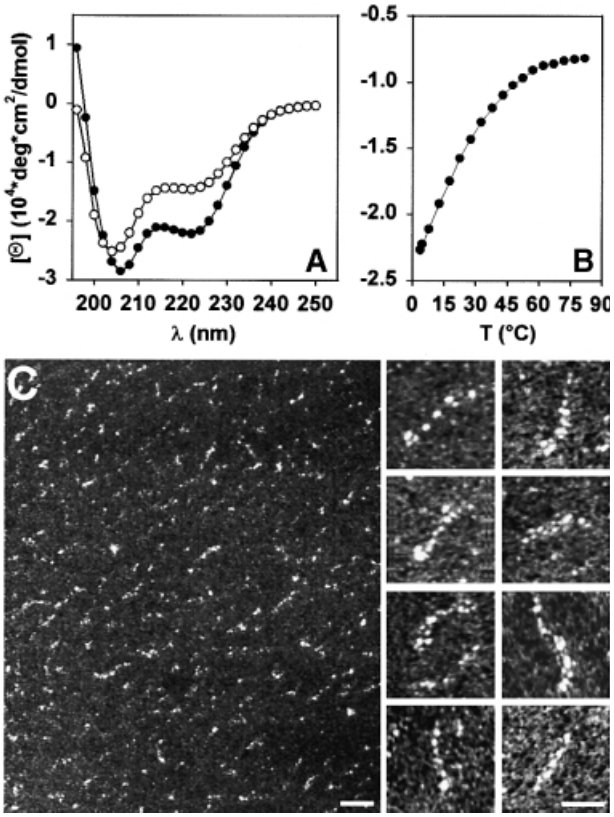

Fig. 1. CD spectroscopy and EM of recombinant human Op18. (**A**) CD spectra recorded at 5°C (●) and 25°C (○). (**B**) Thermal unfolding (●) and refolding (__) profiles recorded at 222 nm. Op18 was adjusted to a concentration of 25 μM in 5 mM sodium phosphate pH 7.4 containing 150 mM NaCl. (**C**) Electron micrographs of glycerol-sprayed/rotary metal-shadowed recombinant Op18 molecules at 20°C. Scale bars, 20 nm for the low magnification overview and 10 nm for the high magnification gallery.

Results

Op18 can fold into a flexible and extended α-helical structure

Far-ultraviolet (UV) CD spectroscopy was employed to probe for the secondary structure of the recombinantly produced and affinity-purified Op18 molecule. As illustrated in Figure 1A, the far-UV CD spectrum recorded at 5°C from Op18 exhibited minima at 207 (α-helix π–$\pi_{\|}$* transition) and 222 nm (α-helix n–π* transition), which is characteristic of proteins with a helical conformation. A helical content of ~60% was estimated from the $[\Theta]_{222}$ value of –23 000 deg × cm^2/dmol, assuming that a value of –37 300 deg × cm^2/dmol corresponds to 100% helicity for a 149 residue polypeptide (Chen *et al*., 1974). This finding is consistent with the secondary structure prediction by the PHDsec algorithm of Rost *et al*. (1994), which predicts a very high degree of α-helicity for all residues from Leu47 to Glu89 and from Phe93 to Asn136. Taking into account that the axial rise per residue in an α-helix corresponds to 0.15 nm, a 90 amino acid residue sequence should fold into an ~14 nm long, extended helical structure.

The stability of the recombinant protein was assessed by a thermal unfolding profile recorded by CD spectroscopy at 222 nm. As shown in Figure 1B, for a concentration of 25 μM, Op18 revealed a broad, non-cooperative transition. The profile indicates that Op18 unfolds rapidly with increasing temperature and is largely denatured by 40°C. The spectra recorded at 25°C revealed a shift in the wavelength of the first minimum from 207 to 204 nm (mixture of α-helix π–$\pi_{\|}$* transition and random coil π–π* transition) and a concomitant decrease of $-[\Theta]_{222}$ consistent with a shift in the equilibrium from helix to random coil (Figure 1A). However, the $[\Theta]_{222}$ value of –15 000 deg × cm^2/dmol, which corresponds to a helical content of ~40%, indicates that at 25°C Op18 is still substantially structured. The thermal unfolding was completely reversible, with 100% of the starting signal recovered upon cooling (Figure 1B), explaining the observation that Op18 remains soluble and active after boiling (Sobel, 1991). The non-cooperative thermal unfolding profile and the $[\Theta]_{222}$:$[\Theta]_{207}$ ratio of <1 suggests the presence of a 'straight' helix rather than a helix that folds back on itself in an antiparallel fashion.

The oligomeric state of the recombinant Op18 molecule was assessed by AUC. At 20°C, sedimentation equilibrium of a 25 μM Op18 solution yielded an average molecular mass of 18.1 kDa. Repetition of the experiment at 4°C yielded an average molecular mass of 16.3 kDa. These values are consistent with a monomeric molecule of Op18 (calculated molecular mass of the monomer, 17.4 kDa). Sedimentation velocity analysis revealed average sedimentation coefficients $s_{20,w}$ of 1.4S and 1.1S at 20 and 4°C, respectively. These values indicate an elongated and temperature-dependent molecular shape of Op18.

Transmission electron microscopy (TEM) was employed to examine further the molecular shape of Op18. As illustrated in the low magnification overview of Figure 1C, inspection of Op18 molecules after glycerol spraying at room temperature and subsequent rotary metal shadowing yielded irregularly shaped and rather heterogeneous appearing particles. This observation is not surprising considering the results obtained by CD, which indicate that Op18 folds into a labile α-helical structure (see above). However, a closer look at several electron micrographs revealed a significant amount of particles with a thin and flexible, rod shaped appearance (see high magnification images of Figure 1C for selected examples).

Taken together, these results suggest that the monomeric Op18 molecule can fold into a flexible and extended α-helical structure, which is in equilibrium with a less ordered structure.

Op18 stabilizes a kinked protofilament-like tubulin tetramer

The activity of the recombinantly produced Op18 was tested using an MT sedimentation assay. As shown in Figure 2A, at near equimolar concentrations, Op18 completely inhibited the polymerization of a 15 μM tubulin solution. As illustrated in Figure 2C, complex formation of Op18 with tubulin could be visualized directly by TEM. In the absence of Op18, tubulin molecules, after glycerol spraying and subsequent rotary metal shadowing, yielded uniformly distributed globular particles, ~8 nm in diameter (Figure 2B). In contrast, inspection of a similar tubulin preparation that was pre-incubated in a 2:1 molar ratio with recombinant Op18 yielded uniformly distributed, predominantly elongated particles of ~8 × 17 nm (Figure 2C). STEM mass measurements (Müller *et al*.,

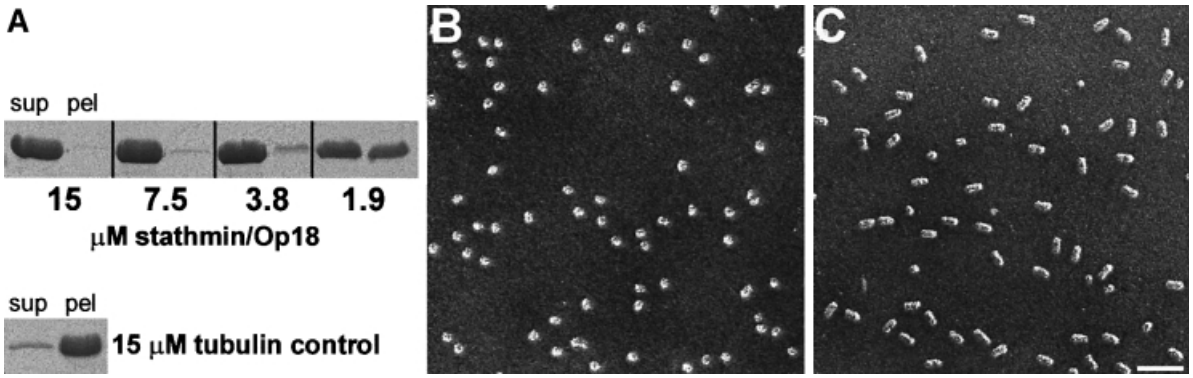

Fig. 2. Tubulin sequestering activity of recombinant Op18. (**A**) Tubulin (15 μM) was incubated with various amounts of Op18 and polymerized to MTs as described in Materials and methods. After high-speed centrifugation, the supernatants (sup) and the pellets (pel) were separated and analysed on SDS–PAGE by Coomassie Blue staining. Only the tubulin protein bands (migrating at ~50 kDa) are displayed. Bottom: tubulin control preparation without Op18. (**B**) TEM electron micrograph of glycerol-sprayed/rotary metal-shadowed tubulin subunits. (**C**) TEM electron micrograph of glycerol-sprayed/rotary metal-shadowed Op18:tubulin complexes. Scale bar for (B) and (C), 50 nm.

1992) of 526 unstained freeze-dried specimens (not shown) yielded an average mass of 197 ± 76 kDa. This value reasonably accounts for the mass of one Op18 and two α/β-tubulin heterodimers, which have previously been reported as components of the complex (Curmi *et al*., 1997; Jourdain *et al*., 1997; Howell *et al*., 1999; Larsson *et al*., 1999b). The large standard deviation is common for particles of this kind and recorded under similar conditions (reviewed by Engel and Colliex, 1993).

To assess further the morphology of the Op18:tubulin complex in detail, we recorded electron micrographs of negatively stained specimens by STEM in the annular dark-field (ADF) mode. As shown in Figure 3A (low magnification overview), the particles appeared fairly homogeneous in overall size and shape. Besides the characteristic elongated and curved conformation, almost all complex particles displayed an asymmetric structure that was due to an apparently thicker tip at one end of the complex (see arrows of the gallery in Figure 3A). For averaging, multivariate statistical analysis (van Heel, 1984) was used to divide the data set comprising 270 angularly and translationally aligned projection images into 20 subclasses each representing a set of mutually similar images. Importantly, the overall dimensions and the apparent curvature of the resulting Op18:tubulin projected average images were very similar in all 20 subclasses. The variation between different classes was due mostly to differences in the delineation of the particle boundary by the heavy metal salt deposition, to differences in the apparent degree of curvature that varied between 18 and 33° with mean and standard deviation values of 25.3° ± 4.7 and to differences in particle inclination relative to the support film. A representative example of an averaged image comprising 23 particles is displayed at the bottom right corner of the gallery in Figure 3A.

As illustrated in Figure 3B, the projected averaged view of the elongated asymmetric and kinked Op18:tubulin revealed a complex of 5.5 × 17.6 nm in dimensions. The averaged particle image exhibited two pairs of centres of mass. The centres of masses are 4 nm apart (see Figure 3B). This corresponds to the tubulin monomer spacing found longitudinally within protofilaments of an MT (for a review, see Mandelkow and Mandelkow, 1995). As

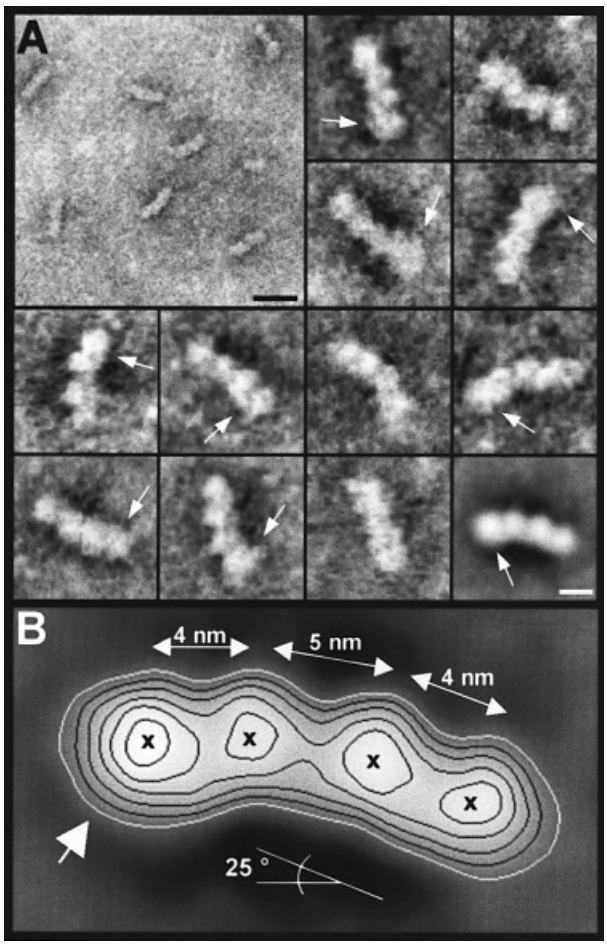

Fig. 3. (**A**) Contrast-reversed STEM ADF electron micrographs of negatively stained Op18:tubulin complexes. Bottom right image: representative average comprising 23 particles of a subclass obtained by multivariate statistical analysis of a set of 270 particles. Arrows point to the slightly thicker appearing tips of the complexes. Scale bars, 20 nm for the low magnification overview and 5 nm for the high magnification images. (**B**) Same average as the bottom right image in (A) displayed enlarged and with isodensity contours superimposed. Crosses mark the centres of mass. The flat (at lower particle radius) and ribbed side (at higher particle radius) suggest that they correspond to the outside and inside, respectively, of the MT wall.

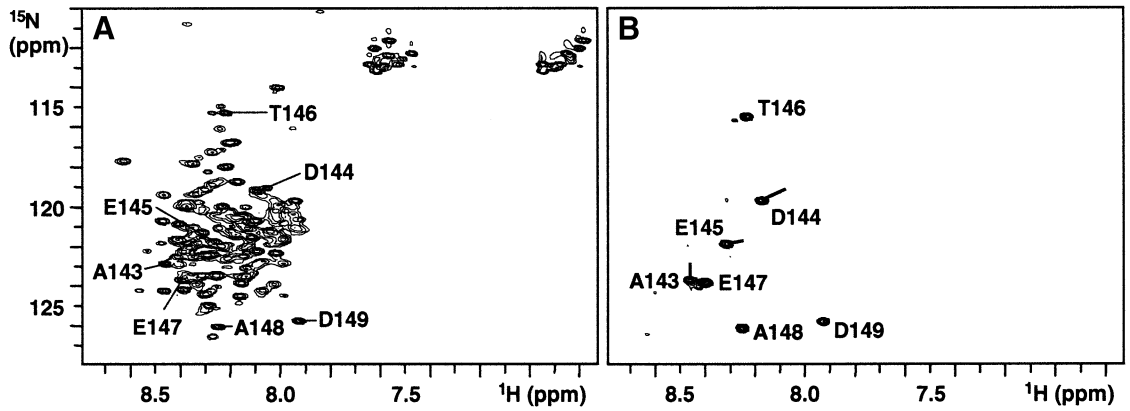

Fig. 4. ^{15}N,^{1}H HSQC spectra of unbound ^{15}N-labelled Op18 (**A**) and tubulin-bound ^{15}N-labelled Op18 (**B**). Assignments are indicated for the seven Op18 residues that are flexible in the Op18:tubulin complex. Lines in (B) indicate resonance shifts for Ala143, Asp144 and Glu145.

indicated by the large white arrow, a slight increase in density was apparent at the tip and towards the flat side of one tubulin monomer. The tubulin dimers were tilted with respect to each other by ~25°, which gives rise to the curved or kinked appearance. The apparent bend between monomers within the tubulin dimer was found to be ~15°. The contact at the subunit interface with a centre-to-centre distance between adjacent monomers of 5 nm was looser than the tight 4 nm contacts within the tubulin dimers (see Figure 3B). The characteristic curved structure of the Op18:tubulin complex has a striking resemblance to the 'relaxed' conformation of a protofilament containing GDP in the exchangeable site of β-tubulin (for review, see Downing and Nogales, 1998). Accordingly, the flat (at lower particle radius) and ribbed side (at higher particle radius) of the Op18:tubulin complex suggest that they correspond to the outside and inside, respectively, of the microtubule wall (Hoenger *et al*., 1995; Nogales *et al*., 1995, 1999).

Taken together, these results demonstrate that Op18 stabilizes an asymmetric and kinked protofilament-like tubulin tetramer.

Most Op18 residues are tightly bound to tubulin in the Op18:tubulin complex

In order to analyse structural changes of Op18 upon binding to tubulin, NMR studies were performed using ^{15}N-labelled Op18 and unlabelled tubulin. The 2D ^{15}N,^{1}H correlation spectrum (HSQC) of unbound Op18 at 25°C (Figure 4A) revealed ~50 sharp backbone N–H resonances, characteristic for unstructured and flexible residues. However, ~90 broader backbone N–H resonances with limited chemical shift dispersion, characteristic for residues that are in rapid exchange between random coil and helical conformations, were observed. When tubulin was added, the ^{15}N-label allowed the selective observation of Op18 in the complex. Due to the large size of the complex (~200 kDa) and its correspondingly slow tumbling in solution, all Op18 residues that are tightly bound to tubulin are expected to broaden beyond distinction and become invisible for NMR. Indeed, most of the resonances disappeared in the HSQC spectrum of the complex, indicating tight binding to tubulin of most Op18 residues (Figure 4B). Seven Op18 backbone amide resonances remained visible in the HSQC spectrum, indicating that these residues were still flexible in the complex. Using heteronuclear 3D NMR experiments, these residues were identified as Ala143–Asp149, the last seven residues of Op18. Asp149, Ala148, Glu147 and Thr146 resonate at very similar frequencies in free and bound Op18, indicating negligible influence from tubulin. Ala143, Asp 144 and Glu145, on the other hand, experienced some chemical shift changes in the complex (lines in Figure 4B), which indicates that these residues are influenced by tubulin, although they are clearly not tightly bound.

Dissecting the function of the N- and C-terminal domains of Op18

It is well known that tubulin can also assemble into linear protofilament-based ring oligomers under certain conditions. Jourdain *et al*. (1997) using AUC demonstrated that Op18 causes dissociation of Mg^{2+}-induced tubulin-GDP ring oligomers at 4°C. Moreover, under solution conditions similar to those leading to MT assembly, they further found that assembly of tubulin:colchicine into ring oligomers and higher aggregates was prevented by Op18 in a manner consistent with the formation of a specific Op18:tubulin:colchicine complex. In agreement with these observations, in the presence of 16 mM $MgCl_2$ and 1 mM GDP at 4°C (Howard and Timasheff, 1986), Op18 either inhibited tubulin-GDP aggregation or dissociated preformed ring oligomers. In both cases, the formation of specific Op18:tubulin complexes was revealed by TEM (Figure 5A) and they appeared very similar to Op18:tubulin complexes obtained under MT polymerizing conditions. Together, these results demonstrate that Op18 inhibits further longitudinal Op18:tubulin complex aggregation.

To test whether the N-terminal part of Op18 is responsible for the inhibition of this aggregation process, an Op18 deletion mutant comprising residues Lys41–Lys140 (referred to as STHM41–140) was prepared by heterologous gene expression in *E.coli*. The fragment, which corresponds to the predicted C-terminal α-helical domain of Op18 (see above), yielded a CD estimated helical content of >70% at 5°C (not shown). At 20°C, sedimentation equilibrium of a 35 μM STHM41–140 solution yielded an average molecular mass of 12.0 kDa (calculated molecular mass of the monomer, 12.1 kDa). This value is consistent with a monomeric conformation of STHM41–140.

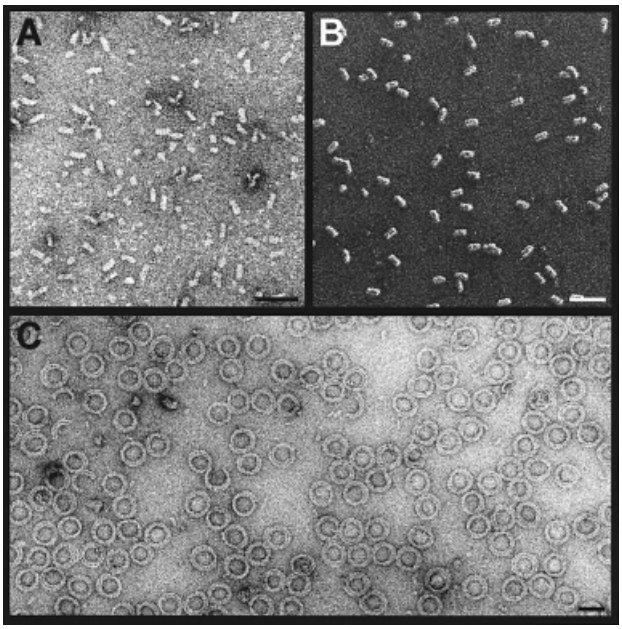

Fig. 5. Functional analysis of the STHM41–140 deletion mutant. (**A**) TEM image of negatively stained Op18:tubulin complexes obtained under double ring-forming conditions (i.e. 16 mM Mg^{2+}, 1 mM GDP, 1 h at 4°C). (**B**) TEM image of glycerol-sprayed/rotary metal-shadowed STHM41–140:tubulin complexes obtained under MT polymerization conditions (i.e. 6 mM Mg^{2+}, 0.5 mM GTP, 3.4 M glycerol, 1 h at 37°C). (**C**) TEM image of negatively stained STHM41–140:tubulin double ring oligomers obtained under double ring-forming conditions as described in (A). For each experiment, 15 μM of tubulin was incubated with equimolar amounts of Op18 or STHM41–140. Scale bars, 50 nm.

Like the wild-type protein, equimolar amounts of STHM41–140 were sufficient to inhibit completely the polymerization of a 15 μM tubulin solution (i.e. in the presence of 6 mM Mg^{2+}, 0.5 mM GTP, 3.4 M glycerol, 37°C). When inspected by TEM, STHM41–140:tubulin complexes appeared very similar in overall size and conformation to Op18:tubulin complexes (compare Figure 5B with Figure 2C). However, in contrast to the full-length Op18 (Figure 5A), the formation of double ring oligomers (i.e. in the presence of 16 mM $MgCl_2$ and 1 mM GDP at 4°C) was not inhibited by the STHM41–140 deletion mutant (Figure 5C). High-speed centrifugation confirmed that STHM41–140 was bound to the pelleted material (not shown). The same results were reproduced in the presence of 10 mM $CaCl_2$ and 1 mM GDP at room temperature (not shown), indicating that formation of STHM41–140:tubulin double rings can be obtained under very different conditions. As illustrated in Figure 5C, the ring-like oligomers revealed a diameter of ~50 nm. They appeared very similar in size and shape to double rings that were obtained under similar conditions from pure tubulin-GDP by Díaz *et al*. (1994). These authors reported bending angles of 30 and 22.5° per tubulin subunit for the inner and outer rings, respectively, which correlates well with the angle found in the Op18:tubulin complex (see above).

Finally, to address whether the length of the C-terminal α-helical domain of Op18 is necessary for stable Op18:tubulin complex formation, we prepared two truncation mutants, STHM41–110 (comprising residues Lys41–Glu110) and STHM76–149 (comprising residues Arg76–Asp149), by heterologous gene expression in *E.coli*. In contrast to the full-length Op18 C-terminal domain (STHM41–140), both truncated fragments completely lost their ability to inhibit the polymerization of a 15 μM tubulin solution (not shown).

Taken together, our results demonstrate that: (i) under MT polymerizing conditions, the α-helical domain of Op18 is sufficient to stabilize tubulin tetramers; (ii) the 40 N-terminal amino acid residues of Op18 are necessary to prevent further longitudinal Op18:tubulin complex aggregation; and (iii) the precise length of the C-terminal α-helical domain of Op18 is necessary to form a stable ternary complex with α/β-tubulin heterodimers. These findings strongly support the suggestion that Op18 stabilizes a protofilament-like tubulin oligomer.

Discussion

It is believed that the balance between MT stabilizing and destabilizing factors is responsible for the observed rapid switching between growth and shrinkage of MTs *in vivo* (Desai and Mitchison, 1997). However, knowledge about MT destabilizing factors is far less advanced than the knowledge about the large group of well-characterized stabilizing microtubule-associated proteins (MAPs). The only known MT destabilizing factors today are the members of the Op18/stathmin phosphoprotein family (reviewed by Gavet *et al*., 1998), the members of the Kin I kinesin subfamily (Walczak *et al*., 1996; Desai *et al*., 1999) and the ATP-dependent MT-severing protein katanin (Hartman *et al*., 1998; Hartman and Vale, 1999). Detailed knowledge on the regulation and on the mechanism of action of MT destabilizing factors is crucial to understand how they affect the dynamic state of MTs during the cell cycle.

Although many *in vitro* and *in vivo* studies on the effects of phosphorylation on tubulin binding have provided important information on Op18 action (for reviews, see Sobel, 1991; Lawler, 1998), the exact mechanism by which Op18 destabilizes MTs is still unresolved. Originally, Op18 was identified as a protein that sequesters tubulin dimers and promotes catastrophes of MTs (Belmont and Mitchison, 1996a). However, Curmi *et al*. (1997) and Jourdain *et al*. (1997) subsequently proposed that Op18 simply acts as a pure tubulin-sequestering protein without significantly interacting with MT ends and regulating their dynamic properties. With our structural approach, we provide new insights into the mechanism of action of Op18 on tubulin and MTs.

Op18 can specifically recognize MT ends to promote catastrophes

One of the key properties of MTs is that of 'dynamic instability' (Mitchison and Kirschner, 1984). Dynamic instability comprises the continuous switching between catastrophes (depolymerization or shrinkage phase) and rescues (polymerization or growing phase) of individual MTs. It is well known that hydrolysis of the GTP bound to the exchangeable site of β-tubulin after polymerization (the GTP bound to α-tubulin is non-exchangeable and never hydrolysed) changes the conformation of a protofilament from a 'straight' tubulin-GTP (i.e. with GTP bound to α- and β-tubulin) to a 'curved' tubulin-GDP

(i.e. with GTP bound to α-tubulin and GDP bound to the β-tubulin) structure (for reviews, see Erickson and O'Brien, 1992; Carlier *et al*., 1997; Desai and Mitchison, 1997). The curved protofilament structure has been documented by cryoelectron microscopic images, which revealed fountain-like arrays of rings that curved away from the MT wall at the fraying ends of depolymerizing MTs (Mandelkow *et al*., 1991). Presumably, the effect of this tubulin-GDP-directed conformational change is to destabilize lateral contacts between adjacent protofilaments within the MT wall, hence inducing catastrophes. Polymerizing MTs are therefore believed to maintain a stabilizing 'cap' of tubulin-GTP subunits whose loss leads to protofilament relaxation and rapid depolymerization. According to Nogales *et al*. (1999), this GTP cap is only formed at the plus end (i.e. fast growing end) of the MT.

Based on the GTP cap model of MTs, one would predict that a protein which induces the curved protofilament conformation should trigger catastrophes. Several lines of evidence suggest that Op18 can act directly on MT ends. Our structural analysis of the Op18:tubulin (Figure 3) and STHM41–140:tubulin (Figure 5) complexes revealed that Op18 stabilizes a kinked protofilament-like tubulin tetramer. NMR spectroscopy of the [^{15}N]Op18:tubulin complex revealed tight binding to tubulin of almost all Op18 residues, including the N-terminus, which is most likely to be unstructured when not bound to tubulin (Figure 4). The data obtained by CD spectroscopy and EM (Figure 1) suggest that the C-terminal domain of Op18 most probably adopts an extended α-helical structure rather than a globular conformation when bound to tubulin. Accordingly, this thin and regularly bound structure is not visible in our 2 nm resolution averaged projection structure of the Op18:tubulin complex (Figure 3B). Nevertheless, as illustrated in Figure 3B, a slight increase in density at the tip and towards the flat side (i.e. which represents the outside surface of the MT wall; Hoenger *et al*., 1995; Nogales *et al*., 1995, 1999) of one tubulin monomer was revealed. According to Nogales *et al*. (1999), this zone of tubulin was found to represent one of the major zones of longitudinal contacts between tubulin subunits within a protofilament. The results obtained with the STHM41–140 fragment showed that, in the absence of the N-terminal part, truncated Op18 promoted formation of protofilament-based double rings (Figure 5). This finding demonstrates that the 40 N-terminal residues of Op18, which most probably accounted for the observed increase in density in the Op18:tubulin complex, is to 'cap' tubulin subunits at a site normally engaged in the formation of longitudinal contacts within protofilaments to ensure the specificity and integrity of the complex. Hence, the C-terminal α-helical domain, which we showed to be sufficient and necessary for specific complex formation (Figure 5B), together with the N-terminal 'capping-domain' of Op18 ideally should allow the molecule to bind along almost the entire length of two longitudinally aligned α/β-tubulin heterodimers at MT ends (Figure 6).

Our structural findings on Op18 and on the Op18:tubulin complex can be combined well with functional studies from the literature. Larsson *et al*. (1999b) carried out a systematic deletion mutant analysis of Op18 and demonstrated that Op18 binds tubulin heterodimers via multiple contacts that span residue 9 through the major part of the molecule. This result supports our structural findings, which suggested that Op18 adopts an elongated conformation when bound to tubulin. Larsson *et al*. (1999a) observed that Op18 induces a significant increase in the low basal GTPase activity of tubulin. More specifically, Larsson *et al*. (1999b) identified three distinct site-dependent levels of modulation of β-tubulin's GTP metabolism: inhibition of nucleotide exchange (mediated by the N-terminal residues 1–46 of the full-length Op18), inhibition of GTP hydrolysis (mediated by the N-terminal residues 46–100 of the α-helical domain) and stimulation of GTP hydrolysis (mediated by the C-terminal residues 100–149 of the α-helical domain). Howell *et al*. (1999) found that Op18 does not destabilize GMPCPP- (a non-hydrolysable GTP analogue) capped MTs. Together, these findings suggest that GTP hydrolysis on β-tubulin is a prerequisite for the catastrophe-promoting activity of Op18. Melander Gradin *et al*. (1997) reported that phosphorylation of Ser16 within the N-terminus is sufficient to reduce the MT-destabilizing activity significantly *in vivo*, and Howell *et al*. (1999), using truncation mutants, found that lack of the first 25 N-terminal residues of Op18 resulted in a protein fragment that retained tubulin-sequestering activity but was unable to promote MT catastrophes. These findings suggest that the N-terminal part of Op18 plays a key role in mediating the MT-destabilizing activity of Op18. In this context, it should be noted that the surface, which is crucial for the formation of longitudinal tubulin contacts within a protofilament, becomes buried within the lattice of the MT wall. However, at the ends of protofilaments, this area remains exposed. Our finding that the N-terminal residues of Op18 bind to this tubulin area together with the necessity to trigger nucleotide hydrolysis on β-tubulin strongly suggests that this part of Op18 is engaged in targeting the molecule specifically to the plus end of an MT in order to promote depolymerization. As a consequence, truncation or phosphorylation of, for example, Ser16 of the N-terminal part abolishes the catastrophe-promoting activity of Op18.

In summary, as illustrated in Figure 6, the structural and functional features of Op18 suggest that, besides its tubulin-sequestering activity, the protein is able to interact directly with the plus end of an MT via multiple binding sites to promote the destabilizing tubulin-GDP-directed conformational change by GTP hydrolysis on β-tubulin.

Comparing the mechanisms of action of MT-depolymerizing factors

Recently, Desai *et al*. (1999) have proposed a preliminary model for the mechanism of MT destabilization by XKCM1/XKIF2, two members of the Kin I kinesin subfamily, and Hartman and Vale (1999) suggested a molecular mechanism for how katanin, a member of the AAA ATPase superfamily, severs MTs. The structural and functional features of Op18 are very distinct from those of XKCM1/XKIF2 and katanin, suggesting that these molecules destabilize MTs by a different mechanism. (i) Op18 is monomeric and exhibits a labile predominantly α-helical structure, whereas XKCM1/XKIF2 are most probably homodimeric molecules with a kinesin-like appearance, and katanin is a heterodimer organized into an enzymatic ring-like subunit and a centrosome-targeting

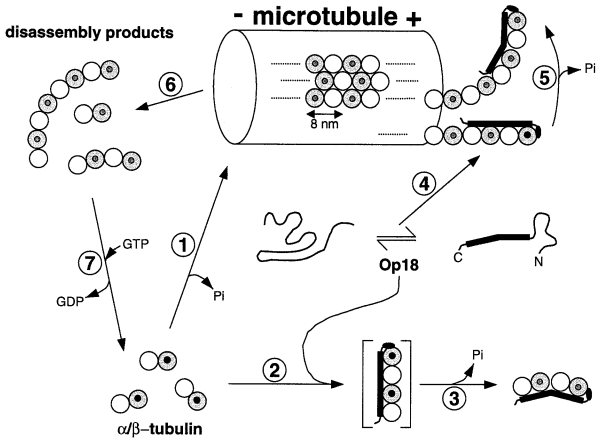

Fig. 6. Proposed mechanism of action of Op18 on tubulin and MTs. On the basis of the results presented here and the biochemical data available from the literature (for details, see Discussion), we derived a possible mechanism of how Op18 acts on tubulin and MTs. Typically, MTs are assembled from tubulin-GTP dimers (1). In the presence of Op18 (which can adopt an extended α-helical structure), assembly of MTs is inhibited. As proposed in (2), a straight intermediate containing four longitudinally aligned tubulin monomers is stabilized by interacting with the entire length of the C-terminal α-helical domain of Op18. Subsequent GTP hydrolysis on β-tubulin, which is stimulated by Op18, induces the preferred tubulin-GDP-driven relaxed conformational change at the inter-dimer interface (3). The resulting kinked Op18:tubulin structure is incompatible with the straight protofilament conformation found within the lattice of the MT wall, making the sequestered tubulins assembly incompetent. The 'cap' formed by the N-terminus of Op18 ensures the specificity and integrity of the complex by preventing further longitudinal Op18:tubulin complex aggregation. Alternatively, Op18 specifically recognizes the plus end of an MT (4). As for tubulin dimers (2), binding of Op18 to a straight tubulin-GTP-capped protofilament promotes GTP hydrolysis on β-tubulin. As a result, the curved and relaxed GDP state protofilament is formed (5). The conformational transition from straight to curved destabilizes the MT, thereby triggering a catastrophe (6). The GDP-containing ring-like MT disassembly products can either be recycled to tubulin-GTP subunits (7) or sequestered by free Op18 molecules. It should be noted that phosphorylation of Op18 on four distinct Ser residues, which regulates the activity of the protein both *in vitro* and *in vivo*, is not considered in the model. White spheres represent α-tubulin and grey spheres β-tubulin. The state of hydrolysis of the nucleotide bound to the exchangeable site of the β-tubulin subunit is indicated by small black (for GTP) or white (for GDP) circles. For simplicity, the non-exchangeable and never hydrolysed nucleotide bound to the α-tubulin subunit is not marked. The minus end of the MT is indicated by (–) and the plus end by (+). All drawings are to scale.

subunit. (ii) XKCM1/XKIF2 and katanin bind and release from tubulin in an ATP-dependent manner, whereas the binding activity of Op18 is tightly regulated by specific phosphorylation events. (iii) Both Op18 and XKCM1/XKIF2 were found to destabilize MTs by targeting directly to MT ends. However, Op18 most likely interacts predominantly at the very plus end of the MT, and activation of the GTPase of β-tubulin is a prerequisite for its catastrophe-promoting activity. In contrast, XKCM1/XKIF2 can promote catastrophes at both the plus and minus end of the MT without the need to induce GTP hydrolysis. Katanin, on the other hand, promotes disassembly of MTs by generating internal breaks (i.e. severing) within an MT.

Conclusions

By all criteria, Op18 most probably represents an authentic MT catastrophe factor with structural and functional features that are clearly distinct from those of the Kin I proteins and katanin. Our structural model (Figure 6) allows the design of new experiments that are necessary to refine and clarify further the exact mechanism by which Op18 regulates MT dynamics *in vivo*. Furthermore, the approach presented here may allow unveiling of the structural basis of Op18 phosphorylation that regulates its activity.

Materials and methods

cDNA library screening and construction of expression plasmids

A human fetal brain cDNA library (Clontech) was used as a template for PCR amplification of the complete coding sequence of the human Op18 gene. At the 5′ end, an *Nde*I site was introduced using the oligonucleotide 5′-CCTCTTCATATGGCTTCTTCTGATATCCAG-3′ as primer. Two TAA stop codons and a *Bam*HI site were introduced at the 3′ end of the coding sequence using the oligonucleotide primer 5′-CCCGGATCCTTATTAGTCAGCTTCAGTCTCGTCAG-3′. The amplified product was ligated into the bacterial expression vector pET-16b (Novagen) at the *Nde*I–*Bam*HI site. For the Op18 fragments, primers were designed to obtain a *Bam*HI site at the 5′ end (STHM41–140 and STHM41–110, 5′-CCCGGATCCAAGAAGAAGGATCTTTCCCTG-3′; STHM76–149, 5′-CCCGGATCCCGAGAGCACGAGAAAGAAGTG-3′) and two TAA stop codons preceding an *Eco*RI site at the 3′ end (STHM41–140, 5′-CCCGAATTCTTATTATTTGGATTCTTTGTTCTT-CCGC-3′; STHM41–110, 5′-CCCGAATTCTTATTACTCTTTATTA-GCTTCCATTTTGTG; STHM76–149, 5′-CCCGAATTCTTATTAGT-CAGCTTCAGTCTCGTCAG-3′). The cloned full-length Op18 cDNA was used as a template for PCR amplification. The PCR product was ligated into the bacterial expression vector pEP-T (Brandenberger *et al*., 1996) at the *Bam*HI–*Eco*RI site. The inserted sequences of the constructs were verified by Sanger dideoxy DNA sequencing.

Bacterial growth, expression, isotopic labelling with ^{15}N and protein purification

The *E.coli* host strain JM109(DE3) (Promega) was used for expression. Bacteria were grown at 37°C in LB medium containing 100 mg/l ampicillin. Isotopic labelling with ^{15}N was performed in modified new minimal medium (Budisa *et al*., 1995). Bacterial cultures were induced at OD_{600} = 0.8 by adding isopropyl-β-D-thiogalactopyranoside (IPTG) to 1 mM and incubating at 37°C for 4 h. Affinity purification of the His_6-tagged fusion proteins by immobilized metal affinity chromatography (IMAC) on Ni^{2+}–Sepharose (Novagen) was performed under non-denaturing conditions at 4°C as described in the manufacturer's instructions. Separation of recombinant human Op18 from the N-terminal His_6 tag by means of an immobilized snake venom prothrombin activator (*Oxyuranus scutellatus* venom from Latoxan) was carried out for 20 h at 4°C as described by Humm *et al*. (1997). Separation of the recombinant STHM41–140, STHM41–110 and STHM76–149 polypeptide chain fragments from the N-terminal His_6-tagged carrier protein by thrombin (Sigma) cleavage was carried out as described by Kammerer *et al*. (1995). Full-length Op18 (corresponding to residues Met1–Asp149) contained one additional His residue, and the fragments STHM41–140, STHM41–110 and STHM76–149 two additional GlySer residues at their N-termini, which are not part of the Op18 sequence.

The homogeneity of the four recombinant Op18 proteins was confirmed by SDS–PAGE and reversed-phase HPLC, and their identity was confirmed by N-terminal amino acid sequence analysis. Concentrations of the purified proteins were determined by the BCA protein assay (Pierce). Unless stated otherwise, all protein samples were dialysed against 5 mM sodium phosphate buffer (pH 7.4) containing 150 mM NaCl and stored at either 4 or –70°C for further analysis.

CD spectroscopy

Far-UV CD spectra and thermal unfolding profiles were recorded on a Jasco J 720 spectropolarimeter equipped with a temperature-controlled quartz cell of 0.1 cm pathlength. The spectra shown are the averages of five accumulations. The data were evaluated with the Jasco J 720 (Japan Scientific) and Sigma Plot (Jandel Scientific) software. A ramping rate of 50°C/h was used to record the thermal unfolding profiles.

AUC

AUC was performed on an Optima XL-A analytical ultracentrifuge (Beckman Instruments) equipped with an An-60ti rotor. The recombinant Op18 molecule and the STHM41–140 deletion mutant were analysed in 5 mM sodium phosphate buffer (pH 7.4) containing 150 mM NaCl, and protein concentrations were adjusted to 0.1–0.8 mg/ml. Sedimentation velocity experiments were performed at 56 000 r.p.m. in a 12 mm epon double-sector cell. Sedimentation coefficients were corrected to water by the standard procedure (Eason, 1986). Sedimentation equilibrium runs were performed at 28 000 r.p.m. for Op18 and at 32 000 r.p.m. for STHM41–140. For all samples, a partial specific volume of 0.73 ml/g was assumed.

NMR spectroscopy

All NMR experiments were carried out at 25°C on a Varian UnityPlus 600 spectrometer operating at 600 MHz proton frequency. For studies on unbound Op18, a 19 mg/ml (1.1 mmol/l) solution of ^{15}N-labelled Op18 in 10 mM sodium phosphate buffer (pH 6.5) was used. For studies on tubulin-bound Op18, a solution containing 50 μM ^{15}N-labelled Op18 and 100 μM tubulin was prepared. ^{15}N,^{1}H HSQC spectra (Bodenhausen and Ruben, 1980) and ^{15}N,^{1}H TROSY spectra (Pervushin *et al*., 1998) were acquired on unbound [^{15}N]Op18 and on the [^{15}N]Op18:tubulin complex. For resonance assignment of [^{15}N]Op18, 3D ^{15}N-edited TOCSY-HSQC using a clean DIPSI-2 mixing sequence, and 3D ^{15}N-HSQC-TOCSY-NOESY-HSQC (Zhang *et al*., 1994) were recorded.

MT sedimentation assay

Pure bovine brain α/β-tubulin (10 mg/ml in 80 mM PIPES pH 6.8, 0.5 mM $MgCl_2$, 1 mM EGTA, 1 mM GTP) was obtained from Cytoskeleton. Tubulin (30 μM) was pre-incubated with various amounts of recombinant wild-type or Op18 fragments (in 50 mM MES–KOH pH 6.8, 0.5 mM $MgCl_2$, 1 mM EGTA) for 30 min at room temperature in a total reaction volume of 50 μl. Polymerization was initiated by adding 50 μl of PBG buffer (50 mM MES–KOH pH 6.8, 1 mM EGTA, 1 mM GTP, 12 mM $MgCl_2$, 6.8 M glycerol) and incubating at 37°C for 1.5 h. MTs were separated from Op18:tubulin oligomers by sedimentation at 300 000 *g* for 15 min at 37°C in an Optima TLX ultracentrifuge (Beckman Instruments). Supernatants and pellets were subjected to SDS–PAGE analysis.

EM, STEM, and digital image analysis and processing

For glycerol spraying/low-angle rotary metal shadowing, 20 μl of protein samples, 0.1–0.3 mg/ml in 5 mM sodium phosphate, 150 mM NaCl pH 7.4, plus 30% glycerol, were sprayed onto freshly cleaved mica at room temperature and rotary shadowed in a BA 511 M freeze-etch apparatus (Balzers) with platinum/carbon at an elevation angle of 3–5° (Fowler and Aebi, 1983). Electron micrographs were taken in a Hitachi H-7000 TEM operated at 100 kV on Kodak SO-163 electron image film at 50 000× nominal magnification, calibrated according to Wrigley (1968).

Sample preparation for STEM mass measurements was according to Müller *et al*. (1992). The freeze-dried, unstained Op18:tubulin complexes were examined at room temperature in the ADF mode. The Vacuum Generator (East Grinstead) STEM HB5 was operated at an accelerating voltage of 80 kV. Digital images comprising 512 × 512 pixels were recorded at a nominal magnification of 200 000× and with an average dose of 345 ± 25 electrons/nm^2. Processing of the STEM data for mass determination was carried out as described previously using the IMPSYS software package (Müller *et al*., 1992).

Negative-stain sample preparations were performed as described by Bremer and Aebi (1994). Op18:tubulin complexes were examined using the STEM, which was operated at 100 kV as described above. Data were recorded with the ADF detector at a nominal magnification of 500 000×. Digital images were analysed and processed using the SEMPER 6 image processing software (Saxton, 1996). Briefly, a total of 270, 64 × 64 pixel fields each containing a single particle within them were extracted from the larger, 512 × 512 pixel images recorded. Angular and translational alignment with respect to a variety of reference images was performed to bring all particles into register with one another. Subsequently, multivariate statistical analysis (van Heel, 1984) was applied for the classification of the aligned particle images so as to define homogeneous subsets for averaging.

Acknowledgements

We are very grateful to Drs U.Aebi and J.Engel for generous technical support. We thank Mr M.Häner and Dr S.A.Müller for excellent technical assistance, and Drs A.Hönger, D.Müller, J.Rahuel, P.Schindler, C.-A.Schönenberger, H.Towbin and H.Voshol for discussions and critical reading of the manuscript.

References

Belmont,L. and Mitchison,T.J. (1996a) Identification of a protein that interacts with tubulin dimers and increases the catastrophe rate of microtubules. *Cell*, **84**, 623–631.

Belmont,L. and Mitchison,T. (1996b) Catastrophic revelations about Op18/stathmin. *Trends Biochem. Sci.*, **21**, 197–198.

Bodenhausen,G. and Ruben,D.J. (1980) Natural abundance nitrogen-15 NMR by enhanced heteronuclear spectroscopy. *Chem. Phys. Lett.*, **69**, 185–189.

Brandenberger,R., Kammerer,R.A., Engel,J. and Chiquet,M. (1996) Native chick laminin-4 containing the β2 chain (s-laminin) promotes motor axon growth. *J. Cell Biol.*, **135**, 1583–1592.

Bremer,A. and Aebi,U. (1994) Negative staining. In Celis, J.E. (ed.), *Cell Biology: A Laboratory Handbook*. Academic Press Inc., London, UK, Vol. 2, pp. 126–133.

Budisa,N., Steipe,B., Demange,P., Eckerskorn,C., Kellermann,J. and Huber,R. (1995) High-level biosynthetic substitution of methionine in proteins by its analogs 2-aminohexanoic acid, selenomethionine, telluromethionine and ethionine in *Escherichia coli*. *Eur. J. Biochem.*, **230**, 788–796.

Carlier,M.-F., Didry,D. and Pantaloni,D. (1997) Hydrolysis of GTP associated with the formation of tubulin oligomers is involved in microtubule nucleation. *Biophys. J.*, **73**, 418–427.

Chen,Y.-H., Yang,J.T. and Chau,K.H. (1974) Determination of the helix and β form of proteins in aqueous solution by circular dichroism. *Biochemistry*, **13**, 3350–3359.

Curmi,P.A., Andersen,S.S.L., Lachkar,S., Gavet,O., Karsenti,E., Knossow,M. and Sobel,A. (1997) The stathmin/tubulin interaction *in vitro*. *J. Biol. Chem.*, **40**, 25029–25036.

Desai,A. and Mitchison,T.J. (1997) Microtubule polymerization dynamics. *Annu. Rev. Cell Dev. Biol.*, **13**, 83–117.

Desai,A., Verma,S., Mitchison,T.J. and Walczak,C.E. (1999) Kin I kinesins are microtubule-destabilizing enzymes. *Cell*, **96**, 69–78.

Díaz,J.F., Pantos,E., Bordas,J. and Andreu,J.M. (1994) Solution structure of GDP-tubulin double rings to 3 nm resolution and comparison with microtubules. *J. Mol. Biol.*, **238**, 214–225.

Di Paolo,G., Pellier,V., Catsicas,M., Antonsson,B., Catsicas,S. and Grenningloh,G. (1996) The phosphoprotein stathmin is essential for nerve growth factor-stimulated differentation. *J. Cell Biol.*, **133**, 1383–1390.

Downing,K.H. and Nogales,E. (1998) Tubulin and microtubule structure. *Curr. Opin. Cell Biol.*, **10**, 16–22.

Eason,R. (1986) Analytical ultracentrifugation. In Rickwood,D. (ed.), *Centrifugation—A Practical Approach*. 2nd edn, IRL Press, Oxford, UK, pp. 251–286.

Engel,A. and Colliex,C. (1993) Application of scanning transmission electron microscopy to the study of biological structure. *Curr. Opin. Biotechnol.*, **4**, 403–411.

Erickson,H.P. and O'Brien,E.T. (1992) Microtubule dynamic instability and GTP hydrolysis. *Annu. Rev. Biophys. Biomol. Struct.*, **21**, 145–166.

Fowler,W.E. and Aebi,U. (1983) Preparations of single molecules and supramolecular complexes for high-resolution metal shadowing. *J. Ultrastruct. Res.*, **83**, 319–334.

Gavet,O., Ozon,S., Manceau,V., Lawler,S., Curmi,P. and Sobel,A. (1998) The stathmin phosphoprotein family: intracellular localization and effects on the microtubule network. *J. Cell Sci.*, **111**, 3333–3346.

Hartman,J.J. and Vale,R.D. (1999) Microtubule disassembly by ATP-dependent oligomerisation of the AAA enzyme katanin. *Science*, **286**, 782–785.

Hartman,J.J. *et al*. (1998) Katanin, a microtubule-severing protein, is a novel AAA ATPase that targets to the centrosome using a WD40-containing subunit. *Cell*, **93**, 277–287.

Hoenger,A., Sablin,E.P., Vale,R.D., Fletterick,R.J. and Milligan,R.A. (1995) Three-dimensional structure of a tubulin–motor-protein complex. *Nature*, **376**, 271–274.

Horwitz,S.B., Shen,H.-J., He,L., Dittmar,P., Neef,R., Chen,J. and Schubart,U.K. (1997) The microtubule-destabilizing activity of metablastin (p19) is controlled by phosphorylation. *J. Biol. Chem.*, **272**, 8129–8132.

Howard,W.D. and Timasheff,S.N. (1986) GDP state of tubulin: stabilization of double rings. *Biochemistry*, **25**, 8292–8300.

Howell,B., Larsson,N., Gullberg,M. and Cassimeris,L. (1999) Dissociation of the tubulin-sequestering and microtubule catastrophe-promoting activities of oncoprotein 18/stathmin. *Mol. Biol. Cell*, **10**, 105–118.

Humm,A., Fritsche,E. Mann,K., Göhl,M. and Huber,R. (1997) Recombinant expression and isolation of human L-arginine:glycine amidinotransferase and identification of its active-site cysteine residue. *Biochem. J*., **322**, 771–776.

Jourdain,L., Curmi,P., Sobel,A., Pantaloni,D. and Carlier,M.-F. (1997) Stathmin: a tubulin-sequestering protein which forms a ternary T_2S complex with two tubulin molecules. *Biochemistry*, **36**, 10817–10821.

Kammerer,R.A., Antonsson,P., Schulthess,T., Fauser,C. and Engel,J. (1995) Selective chain recognition in the C-terminal α-helical coiled-coil region of laminin. *J. Mol. Biol.*, **250**, 64–73.

Larsson,N., Marklund,U., Melander Gradin,H., Brattsand,G. and Gullberg,M. (1997) Control of microtubule dynamics by oncoprotein 18: dissection of the regulatory role of multisite phosphorylation during mitosis. *Mol. Cell. Biol*., **17**, 5530–5539.

Larsson,N., Segerman,B., Melander Gradin,H., Wandzioch,E., Cassimeris,L. and Gullberg,M. (1999a) Mutations of oncoprotein 18/stathmin identify tubulin-directed regulatory activities distinct from tubulin association. *Mol. Cell. Biol*., **19**, 2242–2250.

Larsson,N., Segerman,B., Howell,B., Fridell,K., Cassimeris,L. and Gullberg,M. (1999b) Op18/stathmin mediates multiple region-specific tubulin and microtubule-regulating activities. *J. Cell Biol.*, **146**, 1289–1302.

Lawler,S. (1998) Microtubule dynamics: if you need to shrink try stathmin/Op18. *Curr. Biol*., **8**, R212–R214.

Mandelkow,E. and Mandelkow,E.-M. (1995) Microtubules and microtubule-associated proteins. *Curr. Opin. Cell Biol*., **7**, 72–81.

Mandelkow,E.-M., Mandelkow,E. and Milligan,R.A. (1991) Microtubule dynamics and microtubule caps: a time-resolved cryo-electron microscopy study. *J. Cell Biol.*, **114**, 977–991.

Melander Gradin,H., Marklund,U., Larsson,N., Chatila,T.A. and Gullberg,M. (1997) Regulation of microtubule dynamics by Ca^{2+}/calmodulin-dependent kinase IV/Gr-dependent phosphorylation of oncoprotein 18. *Mol. Cell. Biol*., **17**, 3459–3467.

Melander Gradin,H., Larsson,N., Marklund,U. and Gullberg,M. (1998) Regulation of microtubule dynamics by extracellular signals: cAMP-dependent protein kinase switches off the activity of oncoprotein 18 in intact cells. *J. Cell Biol*., **140**, 131–141.

Mitchison,T.J. and Kirschner,M.W. (1984) Dynamic instability of microtubule growth. *Nature*, **312**, 237–242.

Müller,S.A., Goldie,K.N., Bürki,R., Häring,R. and Engel,A. (1992) Factors influencing the precision of quantitative scanning transmission electron microscopy. *Ultramicroscopy*, **46**, 317–334.

Nogales,E., Wolf,S.G., Khan,I.A., Ludueña,R.F. and Downing,K.H. (1995) Structure of tubulin at 6.5 Å and location of the taxol-binding site. *Nature*, **375**, 424–427.

Nogales,E., Wolf,S.G. and Downing,K.H. (1998) Structure of the αβ tubulin dimer by electron crystallography. *Nature*, **391**, 199–203.

Nogales,E., Whittaker,M., Milligan,R.A. and Downing,K.H. (1999) High-resolution model of the microtubule. *Cell*, **96**, 79–88.

Pervushin,K.V., Wider,G. and Wüthrich,K. (1998) Single transition-to-single transition polarization transfer (ST2-PT) in [^{15}N,^{1}H]-TROSY. *J. Biomol. NMR*, **12**, 345–348.

Rost,B., Sander,C. and Schneider,R. (1994) PHD—an automatic server for protein secondary structure prediction. *Comput. Appl. Biosci*., **10**, 53–60.

Saxton,W.O. (1996) Semper: distortion compensation, selective averaging, 3-D reconstruction and transfer function correction in a highly programmable system. *J. Struct. Biol.*, **116**, 230–236.

Sobel,A. (1991) Stathmin: a relay phosphoprotein for multiple signal transduction? *Trends Biochem. Sci.*, **16**, 301–305.

van Heel,M. (1984) Multivariate statistical classification of noisy images (randomly orientated biological macromolecules). *Ultramicroscopy*, **13**, 165–183.

Walczak,C.E., MitchisonT.J. and Desai,A. (1996) XKCM1: a *Xenopus* kinesin-related protein that regulates microtubule dynamics during mitotic spindle assembly. *Cell*, **84**, 37–47.

Wrighley,N.G. (1968) The lattice spacing of crystalline catalase as an internal standard of length in electron microscopy. *J. Ultrastruct. Res.*, **24**, 454–464.

Zhang,O., Kay,L.E., Olivier, J.P. and Forman-Kay,J.D. (1994) Backbone ^{1}H and ^{15}N resonance assignments of the N-terminal SH3 domain of drk in folded and unfolded states using enhanced-sensitivity pulsed field gradient NMR techniques. *J. Biomol. NMR*, **4**, 845–858.

Received September 3, 1999; revised and accepted December 7, 1999